AJChE 2020, Vol. 20, No. 1, 01 – 10

Fabrication of Cellulose Sponge: Effects of Drying Process and Cellulose Nanofiber Deposition on the Physical Strength

Abdul Halim*[1,4]*
Yinchao Xu[2]
Toshiharu Enomae [3]

[1] *Graduate School of Life and Environmental Sciences, University of Tsukuba, Tsukuba, Ibaraki 305-8572, Japan*

[2] *Department of Light Chemistry Industry, School of Environmental and Natural Resources, Zhejiang University of Science and Technology, Hangzhou, Zhejiang Province, 310023, P.R. China*

[3] *Faculty of Life and Environmental Sciences, University of Tsukuba, Tsukuba, Ibaraki 305-8572, Japan*

[4] *Department Department of Pulp and Paper Technology, Institute of Technology and Science Bandung, Jl. Ganesha Boulevard Lot-A1 Kota Deltamas, Cikarang Pusat, Bekasi, Jawa Barat, 17530, Indonesia*

[*] *e-mail:* abdul-halim.xm@alumni.tsukuba.ac.jp

Cellulose sponge was fabricated by regenerating cellulose from a xanthate solution. The solution, which contained sodium phosphate particles as a template to create sponge porosity, was dried at 55, 65, 75 and 85 °C for 2, 4, 6, and 8 h. During the initial and last stages of drying, mass transfer was controlled in terms of temperature and concentration differences, respectively. The activation energy and pre-exponential factor of the mass transfer coefficient were -51,841.947 kJ mol^{-1} and 7.26×10^{9} m^{-2} h^{-1}, respectively. Regenerated cellulose contained a crystalline type of cellulose II, and the crystallinity was independent of drying conditions. The cellulose was unregenerated at a low drying temperature (T≤55 °C) and short drying period (t≤2h). At higher temperatures and longer drying periods, no relationship between temperature and physical strength was observed. Cellulose nanofiber (CNF) was added to the xanthate solution at a ratio of 1:100 of CNF to linter cellulose for xanthation; however, this did not affect the physical strength of the cellulose sponge for both mechanically and chemically fabricated CNF.

Keywords: Cellulose nanofiber, Cellulose sponge, Drying, Physical strength, Regenerated cellulose

INTRODUCTION

Cellulose is a biomaterial mainly produced by the plant. Its sustainability, abundant availability, biocompatibility, high strength, and zero-carbon footprint

DOI: 10.22146/ajche.51313

lead cellulose as a promising biomaterial. Recently, cellulose sponge has been developed for a more sophisticated purpose, including paper-based copper ion sensor (Xu & Enomae 2017), implants (Märtson et al. 1999), oil-water filter (Halim et al. 2019), temperature-responsive material (Du et al. 2018), lithium battery electrodes, and as a wearable thermoelectric material (Cheng et al. 2018). The methods that have widely been used to fabricate cellulose sponge, including freeze-drying, gas forming, and templating.

For the freeze-drying method, cellulose, or cellulose derivative suspension is pre-treated or directly cooled at a low temperature, and then dried in vacuum conditions. Gustaite et al. (2015) reported regenerated cellulose (RC) from cellulose acetate (CA) using freeze-drying method at -110 °C and has Young's modulus and tensile strength approximately 2.7 N mm^{-2} and 140 kPa, respectively. Freeze-drying pre-treatment recently used is electrospinning. Electrospinning pre-treatment is reported by Xu et al. (2018) to produce a fiber mat from the CA solution. Then, deacetylation using a sodium hydroxide solution in a water-ethanol solvent is conducted to generate RC. RC is then diluted in the solvent before being dried.

The gas-forming method using sodium borohydride has been carried out to generate a porous structure of the RC mat (Joshi et al. 2016). The porous is formed from hydrogen gas released by the reaction of sodium borohydride with water. The RC is then vacuum dried (Joshi et al. 2015).

Recoverable ability, compression stress, and stiffness are the physical properties of cellulose that essential for many applications. For oil-water filter , the cellulose has to be strong enough under a high- pressure condition. As wearable and responsive materials, the cellulose has to be flexible enough to maintain its durability and sensitivity. Porosity and pore size significantly affect the physical properties of cellulose. It is not easy to control the porosity and pore size of a cellulose sponge using the freeze-drying and gas-forming methods than with the templating process. The templating process has been used mainly in porous productions (Wang et al. 2017, Peng et al. 2016, Nandiyanto & Okuyama, 2011). It allows for easy control of either porosity or pore size through the selection of the size and type of a template or process condition. Additives are also used in this method to improve desirable properties such as physical strength.

Cellulose nanofibers (CNF) has been applied as an additive to improve the water retention (Kose et al. 2011) and physical strength of paper (Boufi et al. 2016, Petroudy et al. 2017), or polymer composite (Lee et al. 2018, Sakakibara et al. 2017).

CNF can be fabricated from a bottom-up approach or a top-down approach. A bottom-up fabrication approach produces CNF compounds from a molecular to nano levels, for example, CNF fabrication from xanthate solution (Kubo et al. 2018) or bacterial nano-cellulose (Jozala et al. 2016). While a top-down approach of CNF fabrication reduces the dimension of fibers by chemical or mechanical

treatment, for example, using 2,2,6,6-tetramethyl-piperidine-1-oxyl radical (TEMPO) as a chemical catalyst (Isogai et al. 2011), or mechanically by aqueous counter collision (Kondo et al. 2014).

The prominent physical strength of a CNF-assembled sheet is achieved by abundant hydroxyl groups exposed in the CNF surfaces. Filaments synthesized from a CNF hydrogel by a wet-spinning technique have been reported to have a high tensile strength of 297 MPa and Young's modulus of 21 GPa (Lundahl et al. 2016). An air-dried aqueous counter collision cellulose nanofibers (ACC-CNF) sheet prepared from rice straw cellulose has also shown mechanical properties of 164 MPa in tensile strength, and 4 GPa in Young's modulus (Jiang et al. 2016). However, when CNF was added to a thermomechanical pulp, the authors reported no significant effect in comparison to that of chemical pulp. CNF is aggregated with refined fibers during papermaking and decreased drainage rates under alkaline conditions. Therefore, the effect of CNF's addition to materials requires further research to understand the impact comprehensively . In this research, cellulose sponge was fabricated by heating cellulose regenerated from a xanthate solution. Sodium phosphate was applied as a template to create a porous structure. Here, the effect of drying temperature on the cellulose sponge fabrication was investigated. TEMPO-oxidized cellulose nanofibers (TOCNF) and ACC-CNF were added to a cellulose xanthate solution to fabricate TOCNF- and ACC-CNF-composite sponges, respectively.

MATERIALS AND METHODS

Cellulose Sponge Fabrication

A cellulose sponge was fabricated by mercerizing 4 g linter cellulose powder (Advantec 40-100 mesh, Toyo Roshi Kaisha Ltd., Japan) with 20 g of 20% sodium hydroxide (NaOH) (Fujifilm Wako Pure Chemical Industries Ltd., Japan) in an aqueous solution for 4 h. The mercerized cellulose was then mixed with 4 g of carbon disulfide (CS_2) (Fujifilm Wako Pure Chemical Industries Ltd., Japan) for 2 h followed by adding 26 g of distilled water before being allowed to ripen for 48 h on a rotary mixer. The produced cellulose xanthate solution was mixed with 6 g of sodium phosphate powder ($Na_3PO_4{\cdot}12H_2O$, Fujifilm Wako Pure Chemical Industries Ltd., Japan) as a template for forming pores, and then dried in an oven (Sanyo MIR-262, Japan) for 2, 4, 6 and 8 h at 55, 65, 75 and 85 °C to regenerate the cellulose. The template was subsequently removed by dissolving it with warm water. The resultant sample consisted of two phases: a solid and sponge phase. A drying experiment was performed using 4 ml of cellulose xanthate, which was dried at 55, 65, 75, and 85 °C for 2, 4, 6, and 8 h. The weight of the sample was measured before and after drying. The humidity of the oven atmosphere during drying was measured by a hygrometer (Hygrometer C8, Daiso, Japan).

TOCNF- and ACC-CNF-composite sponges were fabricated by adding 1% aqueous dispersion of TEMPO-oxidized wood pulp-based cellulose nanofiber (Nippon Paper Industries Co., Ltd., Japan)

(Isogai et al. 2011) and 1.32% aqueous dispersion of aqueous counter collision-prepared bamboo-derived cellulose nanofiber (Chuetsu Pulp & Paper Co., Ltd., Japan) (Kondo et al. 2014), respectively, to the xanthate solution (after the 48-h ripening process) and were then stirred on a rotary mixer for 30 min. The mass ratio of CNF to cellulose powder was 1:100. Mixtures were then dried at 65 °C for 6 h.

Characterization

Compression stress measurement was carried out at 23 °C and 50% relative humidity using a compression tester (Force Tester MCT-2150, A&D Co., Ltd, Japan). All cellulose sponge samples were cylindrical and had a height of 10 mm and a diameter of 11 mm. Samples were compressed to 60% of the initial height. The loading and unloading compression rates were both 10 mm/min. The elasticity and toughness of the samples were reflected by the unrecoverable proportion (UP) and the resilient ratio (RR), respectively. The UP and R were calculated according to Eq. (1) and Eq. (2) (Lyu et al. 2017), respectively.

$$\mathrm{UP} = \frac{\varepsilon_b}{\varepsilon_a} \times 100\% \quad (1)$$

$$\mathrm{RR} = \frac{W_b}{W_a} \times 100\% \quad (2)$$

where ε_a is the maximum strain and ε_b is the residual strain when the compression stress drops to zero during the unloading stage. W_a and W_b are the compression works during the compression loading and unloading stages, respectively, are obtained from the area under each stress-strain curve. The porosity was calculated according to Eq. (3).

$$\text{Porosity } (\%) = \frac{V_c - \left(\frac{m_c}{\rho_c}\right)}{V_c} \times 100\% \quad (3)$$

where V_c, m_c, and ρ_c respectively are volume of cellulose sponge, the mass of dry cellulose sponge, and density of cellulose sponge. A structural analysis was carried out using optical microscopy (Olympus SZX10, Japan) and scanning electron microscopy (SEM) (SU-8020, Hitachi High-Technologies Corporation, Japan). X-ray diffraction (XRD) was conducted for cellulose crystalline morphology with an X-ray diffractometer (D8 ADVANCE/TSM, Bruker Corporation, USA) using Cu-Kα with λ=1.5418 Å as a radiation source. The crystallinity index (CI) was calculated according to Eq. (4).

$$CI = \frac{I_c}{I_c + I_a} \times 100\%, \quad (4)$$

I_c is the area under the crystalline peak (020) and I_a is of the area under the amorphous halo.

RESULTS AND DISCUSSION

Drying Kinetics

During drying, the water evaporation rate was affected by mass and heat transfer driven by the concentration and temperature difference, respectively. In the first stage, the difference in temperature between the hydrous sponge and oven induces heat transfer from the environment to the hydrous sponge in different ways. Heat transfer accelerated the mass transfer so that initially, water evaporation occurred rapidly, as shown in Figure 1a.

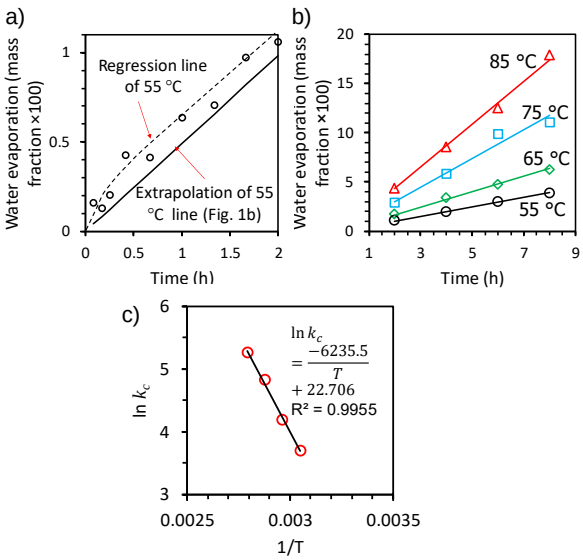

Fig. 1: Water evaporation at 55 °C during initial drying time (a), water evaporation over a duration of 2 h (b), and $\ln k_c$ vs $1/T$ (c)

In the second stage, after the temperature difference became constant, water evaporation became solely driven by the difference in water concentration, i.e., the partial vapor pressure of water. The hydrous sponge's temperature was approximately the same as that of the ambient temperature or a few degrees lower due to the evaporation heat removal. At the bottom, water had a higher fluid density due to a much lower temperature, such that there was no natural convection in this stage. Mathematically, a rate of mass transfer is described by Eqs. (5) and (6) (Geankoplis 1993).

$$J = \frac{dm}{dt} = -k_c A(N_r - N_a) \quad (5)$$

$$m = -k_c A(N_r - N_a)t \quad (6)$$

where J is the mass transfer rate, m is the amount of mass evaporated (mass fraction), t is the elapsed time (h), k_c is the mass transfer coefficient ($m^{-2}h^{-1}$), A is the surface area (m^2), N_r is the concentration of water contained in the sponge (mass fraction), and N_a is the concentration of water in the atmosphere (mass fraction) (see supplementary information for the detail). Eq. (6) implies that the mass of water evaporating during drying bears a linear relationship to time, as shown in Figure 1 (b). A, N_r, and N_a are already known, and k_c is obtained as the gradient of the curve. The convection coefficient value at each temperature is shown in Table 1. The activation energy and pre-exponential factor were calculated by rearranging the Arrhenius equation $k_c = k_0 e^{-E/RT}$ to $\ln k_c = \ln k_0 - E/RT$. Figure 1 (c) shows a plot of $\ln k_c$ to $1/T$. The values of activation energy and pre-exponential factor were -51,841.947 kJ mol^{-1} and 7.26×10^9 m^{-2} h^{-1}, respectively.

Table 1. Mass transfer coefficient (k_c) at various temperatures.

Temperature (°C)	k_c (m^{-2} h^{-1})
55	40.87
65	67.18
75	126.99
85	193.93

Physical Strength

During the drying process, template particles settled down due to the gravitational force, which was higher than buoyancy, and drag force of cellulose xanthate. This process produced a two-phase substance, as shown in Figure 2 (a). The XRD measurement indicated that the regenerated cellulose had a pattern of cellulose II type crystal with peaks around 12°, 20°, and 22° in 2θ corresponding to ($1\bar{1}$ 0), (110), and (020) planes, respectively

(Nam et al. 2016) (Figure 2 (b)). The crystallinity index obtained according to Eq. (4) indicates that this was independent of temperature, as shown in Figure 2 (c). The crystal type transformation from cellulose I to cellulose II occurred during mercerization. The microscopic observation revealed that the cellulose sponges were highly porous (Figure 3). At the lowest drying temperature of 55 °C, the cellulose sponge's structures were more filled than those at higher temperatures. It is because, at low temperatures, some cellulose was regenerated after template dissolution and the structure collapsed. However, the porosity level was similar at all drying temperatures, as shown in Figure 4.

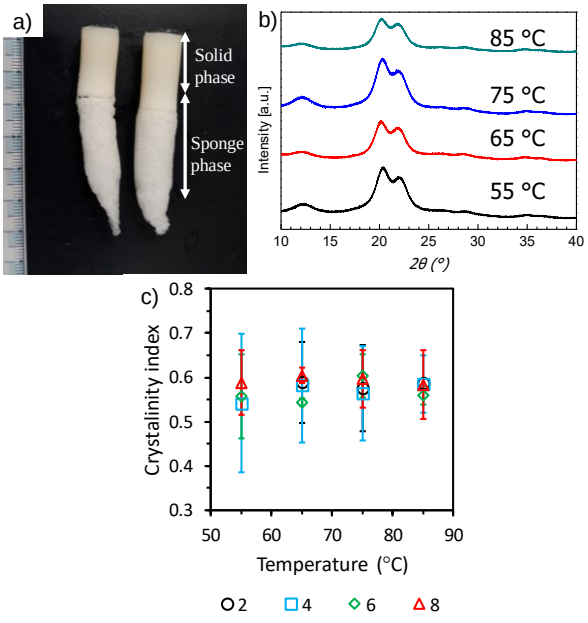

Fig. 2: Photographs (a) and XRD patterns (b) of cellulose sponges at 6 h drying time, and *CIs* (c) of cellulose sponges at various drying times and temperatures

Figure 5 (a) shows the compression stress-strain curves of the cellulose sponges. Three distinct regions have been observed at 55-75 °C: the linear elastic region at ε<10%, the plateau region at 10%<ε<40%, and the densification region at ε>40% (Halim et al. 2019, Cheng et al. 2018). The plateau region is attributed to compression of pores, while the densification region is attributed to the collapse of pores.

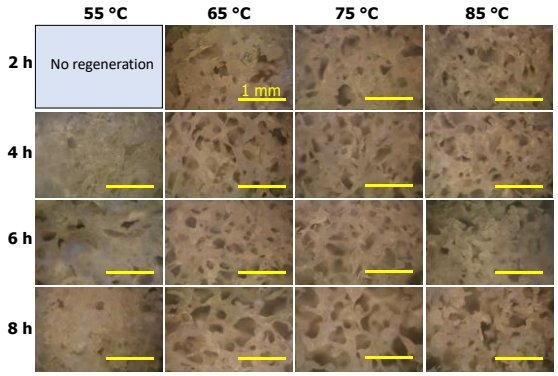

Fig. 3: Optical micrographs of cellulose sponges with no CNF deposited (all scale bars are corresponding to 1 mm)

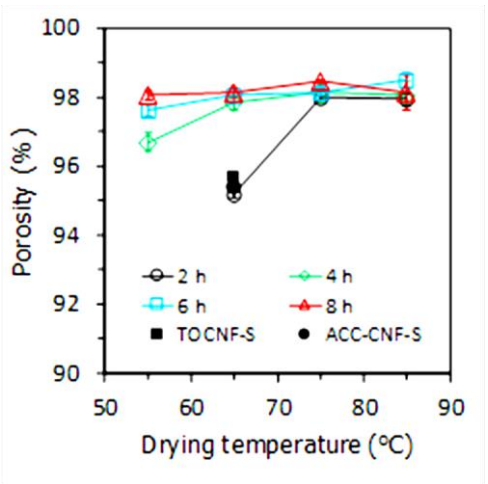

Fig. 4: Porosity of cellulose sponge.

A UP value reflects the elasticity of a cellulose sponge; a highly elastic cellulose sponge will easily recover to the original form after compression and show a low UP value. An RR value reflects the toughness; a tough material will absorb

compression energy without causing fracturing, whereas a brittle material will easily collapse while compression is being applied. Figure 5 (b) shows that there was no relationship between the UP value and drying time and temperature. The regeneration process of cellulose was affected by many factors. Drying temperature affects the water content during the process of regeneration and the Na_3PO_4 dissolution and precipitation; therefore, it is difficult to determine the effect of drying temperature on the UP value. These effects are also applied for the RR value (Figure 5 (c)).

By this physical strength, we utilize the cellulose sponge as a membrane to separate oil and water mixture or methylene blue absorber as reported previously (Halim et al., 2019, Halim et al., 2018). The sponge's high strength is expected to overcome the pressure of the filtration system.

The addition of CNF did not increase the RR or UP values, indicating that CNF did not change the sponge's physical strength. It is because CNF dissolves in xanthate solution with no difference from the pulp-sourced cellulose (Kubo et al. 2018). No cellulose I peak was detected for the CNF-cellulose sponge composite (Figure 6). However, the situation appears more stable at 65 °C in comparison to other drying temperatures. As shown in SEM images, at 65 °C (Figure 7 (b)), the sponge has a more porous structure in comparison to that at 55 °C (Figure 7 (a)) and the CNF composite sponges (Figures 7 (c) and (d)).

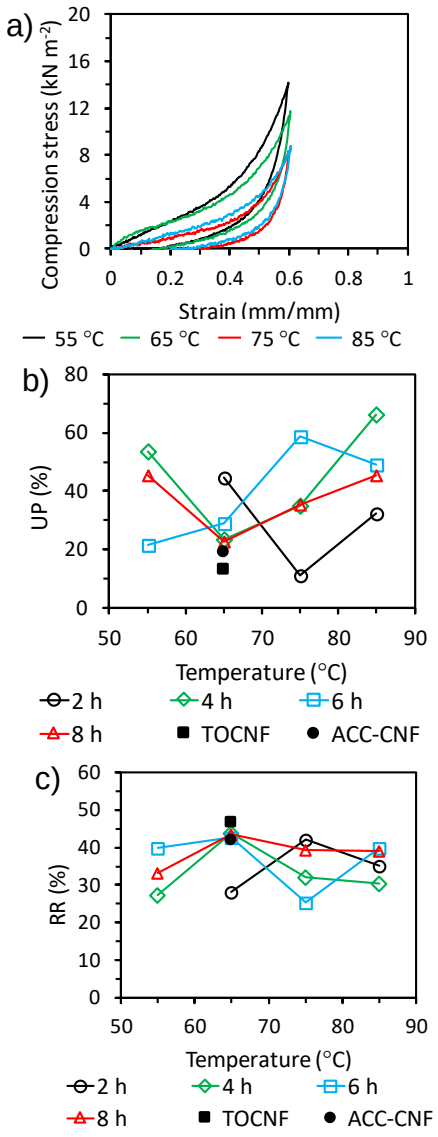

Fig. 5: Compression stress-strain curves for 6 h drying time (a), UP (b), RR (c) of cellulose sponges prepared at different drying temperatures, periods, and CNF additions.

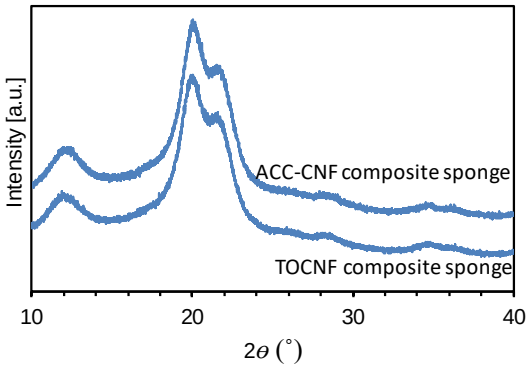

Fig. 6: XRD of CNF composite sponge

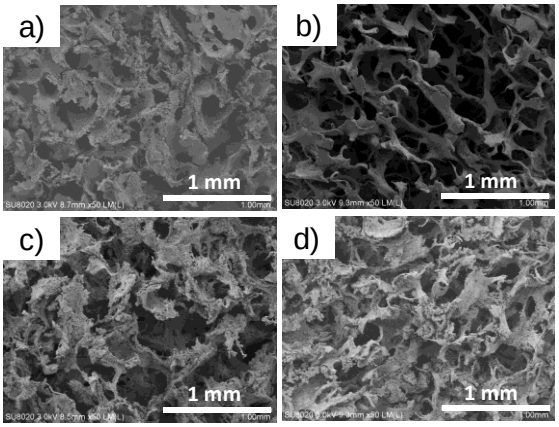

Fig. 7: SEM images of only cellulose sponge obtained after drying at 55 °C for 6 h (a) and at 65 °C for 6 h (b); TOCNF-composite sponge (c); ACC-CNF-composite sponge (d)

CONCLUSION

During drying, the water evaporation rate was affected by heat and mass transfer in the initial stage, whereas it was only affected by mass transfer in the next stage. The activation energy and pre-exponential factors were -51,841.947 kJ mol^{-1} and 7.26×10^{9} m^{-2} h^{-1}, respectively. No relationship was observed between the physical strength of the obtained cellulose sponge and the drying temperature during preparation. The addition of CNF to the xanthate solution did not affect the physical strength of the obtained cellulose sponge. However, a drying temperature of 65 ˚C provided stable physical strength.

ACKNOWLEDGEMENTS

The authors wish to acknowledge Nippon Paper Industries Co., Ltd. and Chuetsu Pulp & Paper Co., Ltd. for providing TOCNF and ACC-CNF, respectively. The nanofab platform of the University of Tsukuba is appreciated for support to observe samples by SEM. JSPS KAKENHI Grant Number 17KT0069 funded this work.

REFERENCES

1. Boufi, S., González, I., Delgado-Aguilar, M., Tarrès, Q., Pèlach, M. À., Mutjé, P. (2016). "Nanofibrillated cellulose as an additive in papermaking process: A review", *Carbohydr. Polym.*, 154, 151-166.
2. Cheng, H., Du, Y., Wang, B., Mao, Z., Xu, H., Zhang, L., Zhong, Y., Jiang, W., Wang, L., Sui, X. (2018). "Flexible cellulose-based thermoelectric sponge towards wearable pressure sensor and energy harvesting", *Chem. Eng. J.*, 338, 1-7.
3. Du, Y., Cheng, H., Li, Y., Wang, B., Mao, Z., Xu, H., Zhang, L., Zhong, Y., Yan, X., Sui, X. (2018). "Temperature-responsive cellulose sponge with switchable pore size: Application as a water flow manipulator", *Mater. Lett.*, 210, 337-340.
4. Geankoplis, C. J. (1993). *Transport processes and unit operations*, Prentice Hall, Englewood Cliffs, New Jersey, U. S. A.
5. Gustaite, S., Kazlauske, J., Bobokalonov, J., Perni, S., Dutschk, V., Liesiene, J., Prokopovich, P. (2015). "Characterization of cellulose based sponges for wound dressings", *Colloids. Surf. A*, 480, 336-342.
6. Halim, A., Xu, Y., Enomae, T. (2018, July 26). "Physical Strength of Cellulose Sponge as Dye Adsorber."

The 9th Asian Symposium on Printing Technology (ASPT2018), Tokyo Big Sight, Tokyo, Japan.
7. Halim, A., Xu, Y., Lin, K-H., Kobayashi, M., Kajiyama, M., Enomae, T. (2019). "Fabrication of cellulose nanofiber-deposited cellulose sponge as an oil-water separation membrane", *Sep. Purif. Technol.*, 224, 322-331.
8. Isogai, A., Saito, T., Fukuzumi, H. (2011). "TEMPO-oxidized cellulose nanofibers", *Nanoscale*, 3, 71-85.
9. Jiang, F., Kondo, T., Hsieh, Y-L. (2016). "Rice straw cellulose nanofibrils via aqueous counter collision and differential centrifugation and Their self-assembled structures", *ACS Sustain. Chem. Eng.*, 4, 1697-1706.
10. Joshi, M. K., Pant, H. R., Tiwari, A. P., Kim, H. J., Park, C. H., Kim, C. S. (2015). "Multi-layered macroporous three-dimensional nanofibrous scaffold via a novel gas foaming technique", *Chem. Eng. J.*, 275, 79-88.
11. Joshi, M. K., Pant, H. R., Tiwari, A. P., Maharjan, B., Liao, N., Kim, H. J., Park, C. H., Kim, C. S. (2016). "Three-dimensional cellulose sponge: Fabrication, characterization, biomimetic mineralization, and in-vitro cell infiltration", *Carbohydr. Polym.*, 136, 154-162.
12. Jozala, A. F., de Lencastre-Novaes, L. C., Lopes, A. M., Santos-Ebinuma, V. D. (2016). "Bacterial nanocellulose production and application: A 10-year overview", *Appl. Microbiol. Biotechnol.*, 100, 2063-2072.
13. Kondo, T., Kose, R., Naito, H., Kasai, W. (2014). "Aqueous counter collision using paired water jets as a novel means of preparing bio-nanofibers", *Carbohydr. Polym.*, 112, 284-290.
14. Kose, R., Kasai, W., Kondo, T. (2011). "Switching surface properties of substrates by coating with a cellulose nanofiber having a high adsorbability", *Sen'i Gakkaishi*, 67, 163-167.
15. Kubo, J., Nakatsubo, T., Ito, K., Tajima, H. (2018). U. S. Pat. US 2018 / 0273644 A1.
16. Lee, J-C., Lee, J-A., Lim, D-Y., Kim, K-Y. (2018). "Fabrication of cellulose nanofiber reinforced thermoplastic composites", *Fiber Polym.*, 19, 1753-1759.
17. Lundahl, M. J., Cunha, A. G., Rojo, E., Papageorgiou, A. C., Rautkari, L., Arboleda, J. C., Rojas, O. J. (2016). "Strength and water interactions of cellulose I filaments wet-spun from cellulose nanofibril hydrogels", *Sci. Rep.*, 6, Article number 30695.
18. Lyu, S., Yang, X., Shi, D., Qi, H., Jing, X., Li, S. (2017). "Effect of high temperature on compression property and deformation recovery of ceramic fiber reinforced silica aerogel composites", *Sci. China Technol. Sc.*, 60, 1681-1691.
19. Märtson, M., Märtson, M., Viljanto, J., Hurme, T., Laippala, P., Saukko, P. (1999). "Is cellulose sponge degradable or stable as implantation material? An in vivo subcutaneous study in the rat", *Biomaterials,* 20, 1989-1995.
20. Nam, S., French, A. D., Condon, B. D., Concha, M. (2016). "Segal crystallinity

index revisited by the simulation of X-ray diffraction patterns of cotton cellulose Iβ and cellulose II", *Carbohydr. Polym.*, 135, 1-9.

21. Nandiyanto, A. B., and Okuyama, K. (2011). "Progress in developing spray-drying methods for the production of controlled morphology particles: From the nanometer to submicrometer size ranges", *Adv. Powder Technol.*, 22, 1-19.
22. Peng, H., Wang, H., Wu, J., Meng, G., Wang, Y., Shi, Y., Liu, Z., Guo, X. (2016). "Preparation of superhydrophobic magnetic cellulose sponge for removing oil from water", *Ind. Eng. Chem. Res.*, 55, 832-838.
23. Petroudy, S. R., Sheikhi, P., Ghobadifar, P. (2017). "Sugarcane bagasse paper reinforced by cellulose nanofiber (CNF) and bleached softwood kraft (BSWK) pulp", *J. Polym. Environ.*, 25, 203-213.
24. Sakakibara, K., Moriki, Y., Yano, H., Tsujii, Y. (2017). "Strategy for the improvement of the mechanical properties of cellulose nanofiber-reinforced high-density polyethylene nanocomposites using diblock copolymer dispersants", *ACS Appl. Mater. Interfaces*, 9, 44079-44087.
25. Wang, Y., Qian, J., Zhao, N., Liu, T., Xu, W., Suo, A. (2017). "Novel hydroxyethyl chitosan/cellulose scaffolds with bubble-like porous structure for bone tissue engineering", *Carbohydr. Polym.*, 167, 44-51.
26. Xu, T., Wang, Z., Ding, Y., Xu, W., Wu, W., Zhu, Z., Fong, H. (2018). "Ultralight electropspun cellulose sponge with super-high capacity on absorption of organic compounds", *Carbohydr. Polym.*, 179, 164-172.
27. Xu, Y., Enomae, T. (2017). "Development of a paper-based sensor for the qualitative and quantitative detection of Cu^{2+} in water", *Nord. Pulp Pap. Res. J.*, 32, 237-243.